Practical Roadmap and Limits to Nanostructured Photovoltaics

Richard R. Lunt, Timothy P. Osedach, Patrick R. Brown, Jill A. Rowehl, and Vladimir Bulović**

The significant research interest in the engineering of photovoltaic (PV) structures at the nanoscale is directed toward enabling reductions in PV module fabrication and installation costs as well as improving cell power conversion efficiency (PCE). With the emergence of a multitude of nanostructured photovoltaic (nano-PV) device architectures, the question has arisen of where both the practical and the fundamental limits of performance reside in these new systems. Here, the former is addressed a posteriori. The specific challenges associated with improving the electrical power conversion efficiency of various nano-PV technologies are discussed and several approaches to reduce their thermal losses beyond the single bandgap limit are reviewed. Critical considerations related to the module lifetime and cost that are unique to nano-PV architectures are also addressed. The analysis suggests that a practical single-junction laboratory power conversion efficiency limit of 17% and a two-cell tandem power conversion efficiency limit of 24% are possible for nano-PVs, which, when combined with operating lifetimes of 10 to 15 years, could position them as a transformational technology for solar energy markets.

1. Introduction

Harvesting sunlight with photovoltaic (PV) cells could generate enough electrical energy to meet the world's increasing energy demand while simultaneously enabling a reduction in the environmental impact associated with present modes of electricity production.[1] Scaling of PV installations to the needed terawatt scale, however, will require significant improvements in the cost-effectiveness of installed PVs, including improvements in their power conversion efficiencies (PCE) as well as reductions in the cost of PV module installation through streamlined fabrication and innovations in rapid and lightweight PV deployment.

Advancements in the field of nanostructured PVs (nano-PVs) have led to rapid improvements over the past decade in the power conversion efficiencies of this broad class of solar cells,[2] in which we include molecular, organic, polymeric, dye-sensitized, and colloidal quantum dot (CQD) PVs due to the similarity of the physical processes that govern their operation and fabrication. In general, we define nano-PVs as solar cells that 1) consist of thin films (<2 μm) of semiconductor material, 2) incorporate nanometer-scale optoelectronic materials that 3) have excitonic or quantum-confinement character and 4) can be fabricated entirely with low-temperature (<300 °C) processing steps. The compatibility of many nanostructured PV materials with the use of low-temperature processing can enable the use of flexible, lightweight substrates,[3,4] potentially leading to a lower cost of solar module fabrication and installation. A particular advantage of nanostructured materials is the tunability of their optical and electronic properties, which may enable the implementation of "third-generation" approaches (i.e., strategies for reducing thermal losses) for improved PV power conversion efficiencies.[5]

Here, we first review the fundamental limits to the performance of solar cells and then consider those limits in the context of various nano-PV technologies that are currently under investigation. We review the state of the art for PV technologies in each material class and calculate practical and semiempirical limits to their efficiency, taking into account the prospect for the application of third-generation concepts such as multiple exciton generation (MEG), singlet fission, and stacked-tandem

Prof. R. R. Lunt
Department of Chemical Engineering and Materials Science
Michigan State University
East Lansing, MI 48824, USA
E-mail: rlunt@msu.edu
Prof. R. R. Lunt, Prof. V. Bulović
Department of Electrical Engineering and Computer Science
Massachusetts Institute of Technology
Cambridge, MA 02139, USA
E-mail: bulovic@mit.edu
T. P. Osedach
School of Engineering and Applied Sciences
Harvard University
Cambridge, MA 02138, USA
P. R. Brown
Department of Physics
Massachusetts Institute of Technology
Cambridge, MA 02139, USA
J. A. Rowehl
Department of Materials Science and Engineering
Massachusetts Institute of Technology
Cambridge, MA 02139, USA

DOI: 10.1002/adma.201103404

device architectures. We also address critical considerations related to cost and module lifetime that are unique to nanostructured PV architectures.

2. Theoretical Limits of PV Operation

Single-junction photovoltaic cells are typically limited by four fundamental loss mechanisms:[6,7] 1) incomplete solar spectrum absorption, 2) thermalization of hot carriers (or excitons) in the form of excess heat, 3) chemical potential (thermodynamic) losses dictating that the photovoltage must be less than band gap (E_G) for relaxed carriers, and 4) radiative recombination. The presence of other non-radiative losses (e.g., Auger recombination,[8] internal or phonon conversion, surface recombination,[8,9] etc.) can further reduce cell performance.[10] Considering only radiative losses, Shockley and Queisser (SQ) predicted a limiting power efficiency of 30% under simulated black body radiation,[7] that has been subsequently recalculated as 33% under AM 1.5 solar irradiance.[6,10]
The power conversion efficiency (PCE) is defined as

$$\eta_P = \frac{J_{SC} V_{OC} FF}{P_0} \quad (1)$$

where V_{OC} is the open circuit voltage, J_{SC} is the short circuit current, FF is the fill factor, and P_0 is the incident power. Starting from the SQ limit, where the ideal diode equation describes the current density (J)–voltage (V) characteristics vis

$$J = \frac{R_P}{R_S + R_P}\left\{J_S\left[\exp\left(\frac{q(V - J R_S)}{nkT}\right) - 1\right] + \frac{V}{R_P}\right\} - J_{SC} \quad (2)$$

where R_P is the shunt resistance, R_S is the series resistance, V is the voltage across the solar cell, J_{SC} is the photocurrent, n is the ideality factor, k is the Boltzmann constant, T is the temperature, and J_s is the reverse saturation dark current. The photocurrent is calculated by convolving the cell photoresponse with the solar spectrum as

$$J_{SC} = q \int S(\lambda) E QE(\lambda) d\lambda \quad (3)$$

where q is the charge of the electron, S is the solar photon flux, and EQE is the external quantum efficiency at wavelength λ. Rearranging Equation 2 for the open circuit condition (when $J = 0$) and assuming that the shunt resistance is very large compared to the series resistance, the V_{OC} can be expressed as

$$V_{OC} = \frac{nkT}{q} \ln\left(\frac{J_{SC}}{J_S} + 1\right) \quad (4)$$

In the SQ limit ($n = 1$), neglecting the photon chemical potential,[11] J_S is determined by radiative recombination as[7]

$$J_S \cong qg \int_{E_G}^{\infty} \frac{E^2 E QE}{\exp(E/nkT) - 1} dE \quad (5)$$

where $g = 2\pi/(c^2h^3)$, c is the speed of light, and h is Plank's constant. Correspondingly, the FF is (for $n = 1$ and $R_P \to \infty$):

Richard R. Lunt earned his PhD from Princeton University and then worked as a post-doctoral researcher at the Massachusetts Institute of Technology (MIT) in the Organic and Nanostructured Electronics Laboratory. Currently, he is an Assistant Professor at Michigan State University where he heads the Molecular and Organic Electronics group. His research interests include organic epitaxy, excitonic photophysics, and thin-film photovoltaics.

Vladimir Bulović is a Professor of Electrical Engineering at MIT, leading the Organic and Nanostructured Electronics Laboratory and co-directing the MIT-ENI Solar Frontiers Center. His interests include studies of physical properties of organic and organic/inorganic nanocrystal composites, and development of novel optoelectronic organic and hybrid nanoscale devices.

$$FF = \frac{J_M V_M}{J_{SC} V_{OC}} \approx \left(\frac{q V_{OC}/kT - \ln(1 + q V_{OC}/kT)}{1 + q V_{OC}/kT}\right)\left(1 - \frac{J_{SC} R_S}{V_{OC}}\right) \quad (6)$$

where $J_M V_M$ is the maximum power operating point on the J–V curve and the resistance term is neglected in the SQ limit.

3. Practical Demonstrations of Nano-PVs Operation

We now consider how the operating parameters for a broad range of reported nano-PV structures compare with these theoretical limits. **Figure 1** and **2** are plots of J_{SC}, V_{OC}, and η_P as a function of the optical gap.[12] This data is also tabulated in **Table 1**.While not exhaustive, this list provides a representative range of efficiencies for each nano-PV type, including the presently highest-reported and certified values.

Five decades since Shockley and Queisser derived the power conversion efficiency limit of single-junction photovoltaic cells, researchers have still not demonstrated such high performance for any photovoltaic device system.[10] For example, the power conversion efficiency of the best single-crystal-Si single-junction PVs is $\eta_P = 25\%$ (without solar concentration),[2,10] which is only

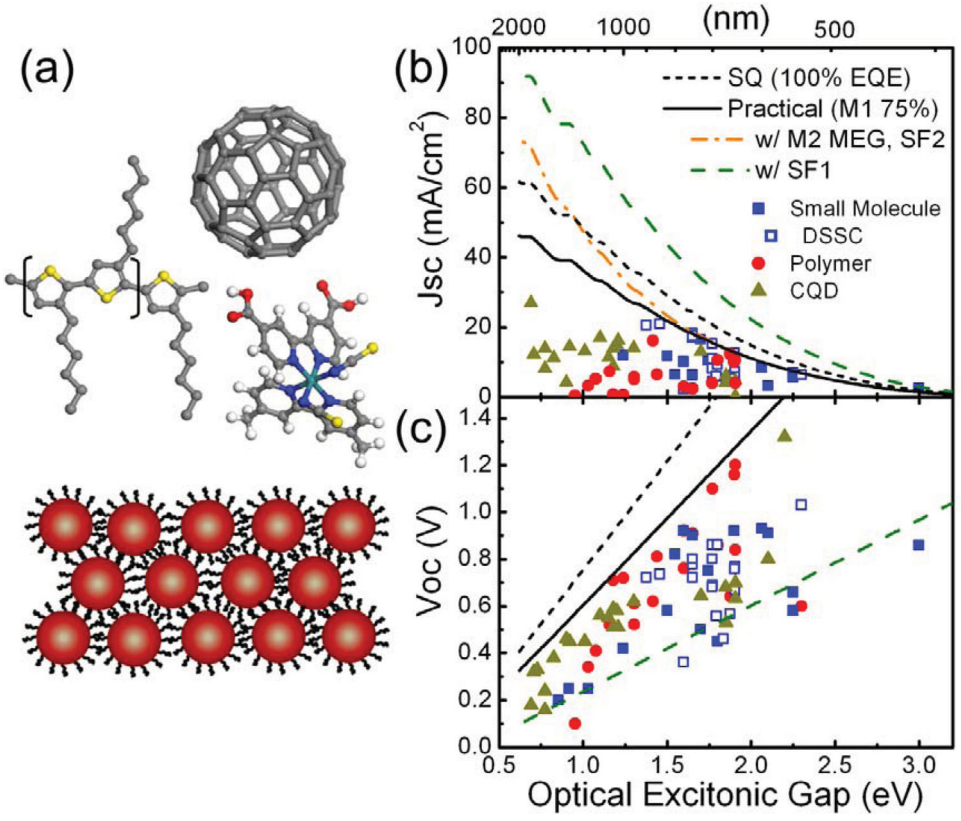

Figure 1. Illustrated structure of nanostructured materials including a) small molecule (C_{60}), organic (Ru-complex), and polymer (P3HT) materials along with ligand-coated CQDs. Calculations of the SQ, practical, and various MEG characteristics of b) photocurrent (J_{sc}) and c) open circuit voltage (V_{OC}) under AM 1.5G illumination as a function of optical or excitonic gap. Note that the V_{OC} for the M1 and M2 MEG cases are nearly identical (the M2 line is therefore emitted for clarity). A range of measured device performance is shown for organic small molecule, dye-sensitized solar cell (DSSC), polymer, and CQD where the gap was estimated from the photoresponse edge (±0.1 eV). The maximum reported photocurrents under AM 1.5G illumination follow the curve for the practical photocurrent limit (M1) defined by 75% *EQE* across the spectrum to E_G. M2 MEG is a two-staircase multiplication, SF1 is a lone singlet fission material (or paired with a bandgap larger than the triplet level), and SF2 is a singlet-fission material paired with acceptor that has an optical gap equal to the triplet level of the SF material.

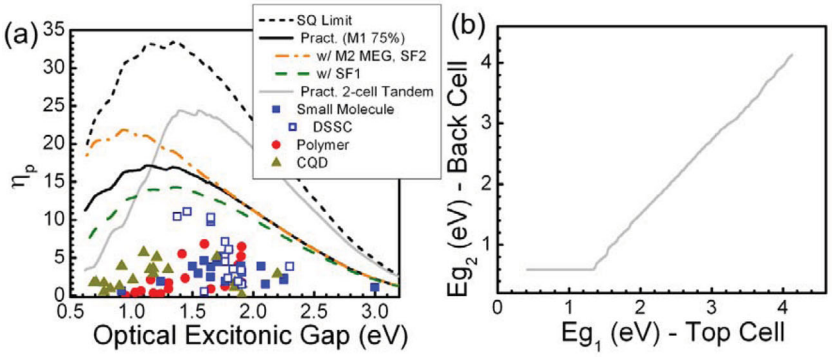

Figure 2. a) Calculations of the SQ, practical, MEG, SF, and two-cell tandem power conversion efficiency (η_P) under AM 1.5G illumination versus optical gap or front-cell gap. A range of measured device performance is shown for organic small molecule, DSSC, polymer, and CQD. b) Calculation of the optimum bandgap pairing for the two-cell tandem as function of top (front)-cell optical gap.

76% of the SQ limit. Hence, in evaluating the achievable performance of a comparatively new PV technology, such as nano-PVs, it is prudent and necessary to make an estimate of the upper limit of the achievable η_P by numerically evaluating trends of the best technical demonstrations. Our literature survey of nano-PV technologies (Table 1) collects device data of the best experimentally reported performance in terms of *EQE*, *FF*, and V_{OC} over the last two decades. From this data a semiempirical estimate for the practical upper limit to the power conversion efficiency of nano-PVs is derived. For example, the maximum demonstrated *EQE* across the spectrum is ≈75% with internal quantum efficiencies approaching 100% (Table 1); the losses in *EQE* are due primarily to combined optical losses (≈10% loss from the transparent conductive oxide electrode absorption, ≈5% reflection from the front facet of the substrate, and ≈10% loss from internal reflections), which likely will be difficult to eliminate in a practical device structure. Assuming this average maximum *EQE* of 75% is maintained at wavelengths extending to the band edge of the optically active semiconductor of the PV cell, upper limits of J_{SC} are calculated as a function of optical bandgap (labeled "M1") according to Equation 3. For estimates of

Table 1. Representative device performance of various single-junction nanostructured photovoltaic cells under 1-sun illumination.

Donor[a)]	Acceptor	E_G [eV]	V_{OC} [V]	J_{SC} [mA cm^{-2}]	*FF*	η_P [%]	Ref.
Small Molecule							
NPD	C_{60}	3.0	0.86	2.5	0.51	1.1	[125]
Tetracene	C_{60}	2.3	0.58	7.0	0.57	2.3	[126]
PtOEP	C_{60}	2.3	0.66	5.6	0.57	2.1	[127]
DIP	C_{60}	2.1	0.93	8.4	0.74	3.9	[128]
Rubrene	C_{60}	2.1	0.91	3.2	0.53	1.5	[129]
DBP	C_{60}	1.9	0.92	6.3	0.65	3.6	[130]
PtTPBP	C_{60}	1.8	0.69	4.5	0.63	1.9	[131]
CuPc	C_{60}	1.7	0.50	16.5	0.56	4.5	[132]
SubNc	C_{60}	1.7	0.79	6.1	0.49	2.5	[133]
BP	Ind-C_{60}	1.7	0.75	10.5	0.65	5.2	[134]
DCV6T	C_{60}	1.7	0.90	6.5	0.64	3.8	[135]
SQ	$PC_{70}BM$	1.6	0.92	12.0	0.5	5.5	[15]
ZnPc	C_{60}	1.5	0.58	11.7	0.62	3.9	[136]
ClAlPc	C_{60}	1.5	0.82	6.5	0.58	3.0	[137]
SnPc	C_{60}	1.2	0.42	7.6	0.63	1.9	[138]
PT Psub	C_{60}	1.0	0.25	–	–	–	[139]
PT Pfused	C_{60}	0.9	0.20	–	–	–	[139]
CNT	C_{60}	0.9	0.25	–	0.51	0.6	[39]
DSSC							
D131	TiO_2, P3HT HTL	2.3	1.03	6.3	0.60	3.9	[140]
Zn5S	TiO_2	1.9	0.67	7.2	0.67	3.1	[141]
Cu-Complex 1	TiO_2	1.9	0.57	5.3	0.64	1.9	[142]
Ru-TPA-NCS	TiO_2,HTL	1.9	0.77	5.7	0.34	1.5	[143]
Ru-TPD-NCS	TiO_2,HTL	1.9	0.76	12.7	0.35	3.4	[143]
Ru Complex	TiO_2	1.8	0.68	15.3	0.69	7.1	[144]
K68	TiO_2	1.8	0.86	11.0	0.68	5.1	[145]
TCPP	TiO_2	1.8	0.46	–	0.62	3.5	[146]
Cu-Complex 1	TiO_2	1.8	0.56	5.9	0.70	2.3	[142]
C101	TiO_2,spiro-MeOTAD	1.8	0.80	8.2	0.69	4.5	[48]
D149	TiO_2, PEDOT HTL	1.8	0.86	9.3	0.75	6.1	[52]
RuL2(SCN)2	TiO_2	1.7	0.72	18.2	0.73	10.0	[147]
CYC-B6S	TiO_2	1.7	0.78	19.8	0.63	9.7	[148]
Ru-Complex	TiO_2	1.7	0.80	17.0	0.74	10.1	[43]
A6141	TiO_2	1.7	0.80	17.6	0.73	10.3	[45]
ZnPcTyr	TiO_2	1.6	0.36	2.3	0.67	0.5	[149]
Black Dye	TiO_2	1.5	0.74	20.9	0.72	11.1	[150]
RuL(NCS)3	TiO_2	1.4	0.72	20.5	0.70	10.4	[44]
Polymer							
P3HT	$PC_{70}BM$ -TiO2	1.9	0.64	12.4	0.51	4.1	[49]
P3HT	PCBM	1.9	0.64	11.3	0.69	5.2	[120,151]
APFO-3	$PC_{70}BM$	1.9	1.16	10.0	–	–	[152]
P3HT	Indene-C_{60}	1.9	0.84	10.6	0.73	6.5	[153]
F8TBT	P3HT	1.9	1.20	4.0	–	1.8	[31]
PCDTBT	$PC_{70}BM$	1.8	0.86	10.6	0.64	6.0	[154]

Table 1. Continued

Donor[a)]	Acceptor	E_G [eV]	V_{OC} [V]	J_{SC} [mA cm^{-2}]	*FF*	η_P [%]	Ref.
F8TBT	PCBM	1.8	1.10	4.0	–	1.3	[31]
PFDPP2T-c	PCBM	1.7	0.91	2.4	0.40	0.9	[155]
PBDTTT-CF	PCBM	1.6	0.76		0.66	6.8	[33]
MDMO-PPV	PCBM	1.6	0.92	3.0	–	–	[152]
PCPDTBT	$PC_{70}BM$	1.4	0.62	16.2	0.55	5.5	[156]
APFO-9	PCBM	1.4	0.81	6.5	0.44	2.3	[30]
PCPDTDPP2T-c	PCBM	1.3	0.61	5.7	0.49	1.7	[155]
P1TPQ	PCBM	1.2	0.71	0.8	0.58	0.3	[32]
P3TPQ	$PC_{70}BM$	1.2	0.52	7.3	0.54	2.1	[32]
PTBEHBQ	PCBM	1.2	0.72	0.6	0.53	0.2	[157]
P3	PCBM	1.1	0.41	5.2	0.29	0.6	[158]
LBPP1	PCBM	1.0	0.34	3.3	0.34	0.4	[159]
PBTTQ	PCBM	1.0	0.10	0.3	0.35	0.01	[160]
CQD							
PbS	–	2.2	1.32	–	0.42	2.9	[161]
CdSe	–	2.1	0.80	–	–	–	[162]
CdSe	–	1.9	0.53	6.2	0.53	1.8	[163]
CdSe QD	–	1.9	0.70	0.2	0.40	0.1	[164]
CdSe TP	–	1.9	0.63	4.8	0.52	1.5	[164]
CdSe NR	–	1.8	0.68	4.2	0.38	1.1	[164]
Sb_2S_3	TiO_2,P3HT	1.7	0.65	13.0	0.61	5.13	[54]
PbS	–	1.2	0.55	11.4	0.56	3.5	[62]
PbS	–	1.2	0.59	8.9	0.56	2.9	[64]
PbS	–	1.2	0.51	16.2	0.58	5.1	[165]
PbS	–	1.2	0.51	14.0	0.51	3.6	[166]
PbS	–	1.2	0.58	15	0.42	3.5	[167]
PbS	–	1.1	0.56	17.0	0.61	5.7	[63]
PbS	–	1.0	0.45	13.2	0.35	2.1	[165]
PbS	–	0.9	0.45	14.5	0.60	3.9	[62]
PbS	–	0.9	0.46	4.2	0.62	1.3	[69]
PbS	–	0.8	0.16	8.2	0.38	0.5	[69]
PbS	–	0.8	0.24	14.0	0.50	1.7	[69]
PbS	–	0.8	0.38	11.3	0.21	0.9	[165]
PbSe	–	0.7	0.18	27.0	0.35	1.7	[68]
PbS	–	0.7	0.33	–	–	–	[168]
PbS	–	0.7	0.32	12.3	0.44	1.8	[168]

[a)]Chemical abbreviations: NPD - *N,N′*-diphenyl-N,N'-bis(1-naphthyl)-1,1′biphenyl-4,4′′ diamine; PtOEP - 2,3,7,8,12,13,17,18-octaethyl-21H,23H-porphine platinum(II); DIP - di-indenoperylene; DBP - dibenzo{[f,f'] - 4,4′,7,7′-tetraphenyl}diindeno[1,2,3-cd:1′,2′,3′-lm]perylene; PtTPBP - platinum tetraphenylbenzoporphyrin; CuPc - copper phthalocyanine; SubPc - boron subphthalocyanine; BP - tetrabenzoporphyrin; DCV6T - bis-(dicyanovinylen)-sexithiophene; SQ - 2,4-bis[4-(*N,N*-diisobutylamino)-2,6-dihydroxyphenyl]squaraine; ZnPc - zinc phthalocyanine; ClAlPc - chloro-aluminum phthalocyanine; SnPc - tin phthalocyanine; PT Psub - diporphyrin–pyrene; PT Pfused - pyrene-fused diporphyrin; CNT - carbon nanotube; P3HT - poly(3-hexylthiophene); APFO-3 - poly[(9,9-dioctylfluorenyl-2,7-diyl)-alt-5,5-(40,70-di-2-thienyl-20,10,30-benzothiadiazole)]; F8TBT - poly((9,9-dioctylfluorene)-2,7-diyl-alt-[4,7-bis(3-hexylthien-5-yl)-2,1,3-benzothiadiazole]-2′,2″-diyl); PBDTTT-CF - poly[4,8-bis(2-ethylhexyloxy)-benzo[1,2-b:4,5-b′]dithiophene-2,6-diyl-alt-(4-octanoyl-5-fluoro-thieno[3,4-b]thiophene-2-carboxylate)-2,6-diyl]; MDMO-PPV - poly[2-methoxy-5-(3′,7′-dimethyloctyloxy)-1,4-phenylene vinylene]; PCPDTBT - poly[2,1,3-benzothiadiazole-4,7-diyl[4,4-bis(2-ethylhexyl)-4H-cyclopenta[2,1-b:3,4-b']dithiophene-2,6-diyl]; P3 - 6,7-diphenyl-4,9-bis-(thiophen-2-yl)-[1,2,5]thiadiazolo[3,4-g]quinoxaline/9-triarylamino-9H-carbazole; PCBM - [6,6]-phenyl-C61-butyric acid methyl ester; spiro-OMeTAD - (2,2(,7,7(-tetrakis-(N,N-di-pmethoxyphenylamine)9,9(-spirobifluorene); PEDOT - poly(3,4-ethylenedioxythiophene); HTL - hole transport layer.

the best practical device performance, upper limits for the *FF* as a function of optical gap are similarly assumed to be that of the highest reported (i.e., *FF* = 0.75) across the spectrum (Table 1). Deviations in *FF* from the SQ limit generally stem from a combination of large series resistance (R_S) and low shunt resistance (R_P). While many empirical forms have been proposed for the dependence of V_{OC} as a function of E_G,[13,14] it is found that maximum demonstrated photovoltages follow a trend of reaching 80% of the value predicted by the SQ limit (Equation 4); the difference can be attributed to a number of recombination phenomena including internal conversion, interface recombination, and exciton binding losses, as discussed below.[15] Nonetheless, this threshold in V_{OC} is consistent with the framework of the SQ limit and can be used in combination with the practical upper limits in photocurrents and fill-factors to estimate the ultimate laboratory efficiency limits of nano-PVs, as shown in Figure 2a. We find that a semiempirically derived maximum efficiency of 17% is achievable for a single-junction cell with a bandgap in the range of 1.1 eV to 1.4 eV. This maximum efficiency is lower than that reported in recent semitheoretical studies in which practical considerations described above are not taken into account and which led to maximum exciton-limited efficiencies ranging from 22–27%.[15] Also plotted in Figure 2a are η_P versus. bandgap curves calculated with Equation 3–5 based on the implementation of various third-generation concepts (shown in **Figure 3**) that will be described in detail below; for two-cell current-matched nanostructured tandems, the optimal efficiency as function of top-cell bandgap is shown in Figure 2a, where the corresponding optimal pairing of the back-cell gap is plotted in Figure 2b.

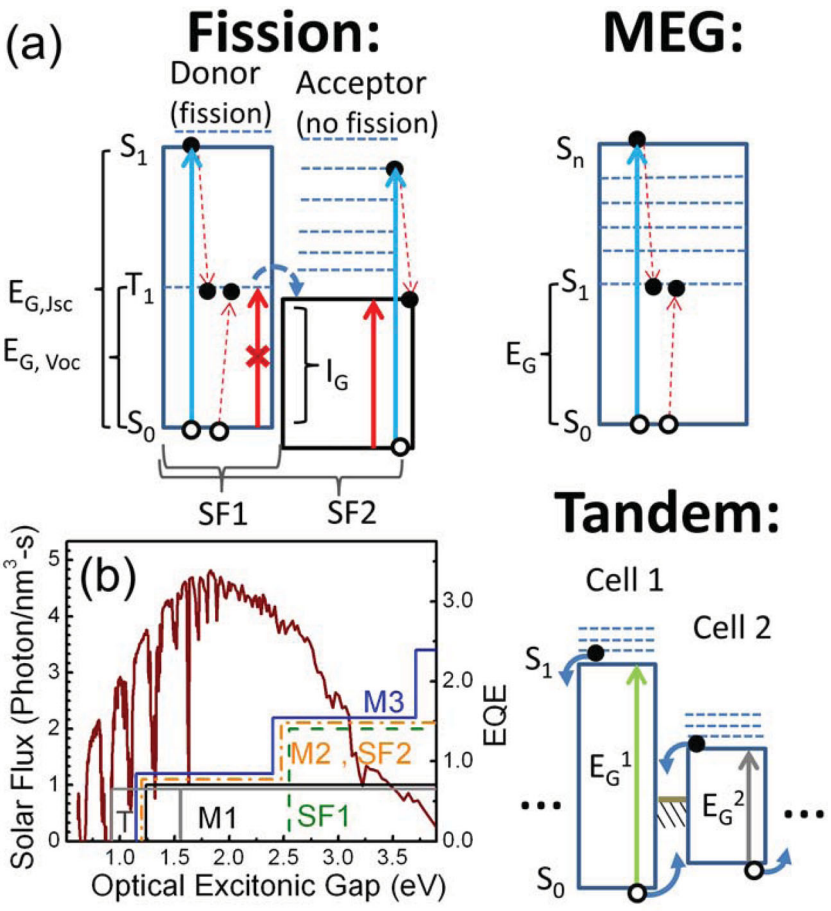

Figure 3. a) Schematic of various methods relevant in nanostructured materials to reduce thermal losses including singlet exciton fission, multiple exciton generation, and tandem stacking. $E_{G,Jsc}$ (singlet level) and $E_{G,Voc}$ (triplet level) are the gaps used to calculate the J_{sc} and V_{OC} in the SQ limit, respectively, for singlet fission case SF1, where there is negligable oscillator strength between the triplet and singlet levels for photocurrent generation. Solid arrows are optical transition, red dashed arrows are electronics transistions associated with multiple exciton generation and the blue dashed line designates charge transfer exciton dissociation. b) AM 1.5G solar photon flux as a function of energy and the representative external quantum efficiency profiles of various cell configurations. Profiles are offset slightly from the M1 (practical) line for clarity; M2 and M3 MEG are a two-staircase and three staircase multiplication profile, respectively; SF1 is a lone singlet fission material (or paired with an acceptor bandgap larger than the triplet level) and SF2 is a singlet-fission material paired with acceptor that has an optical gap equal to the triplet level of the SF material; T is the 2-cell current-matched tandem scenario where the vertical lines indicate the two bandgaps.

4. Analysis of Performance of Nano-PV Technologies

In the remainder of this article, we review the challenges associated with each type of nano-PV device and suggest particular areas for improvement in order to approach the efficiency limits. We then discuss third-generation concepts particularly relevant to nanostructured materials that can allow for efficiencies beyond the single-junction limit and, finally, consider these efficiency limits in the context of the nano-PV module cost and operating lifetime.

4.1. Small Molecule and Polymer PVs

One of the distinguishing features of molecular, organic, and polymeric semiconductors is the presence of strongly bound excited states, known as Frenkel excitons.[16] These excitons have a significant impact on many of the processes in photovoltaic devices, from photocurrent generation to the characteristically pronounced absorption features.[3] For example, organic semiconductors typically exhibit static dielectric constants in the range of 2 to 5[16] and, accordingly, exhibit large exciton binding energies of between 0.2 eV and 0.8 eV.

To overcome this exciton binding energy, bilayer donor–acceptor architectures have become common to promote exciton separation to free carriers[17–19] as shown in **Figure 4**. However, there still remains an inherent tradeoff between the light absorption efficiency within the nano-PV device layers (quantified by the absorption constant, α) and exciton diffusion efficiency (quantified by the exciton diffusion length,

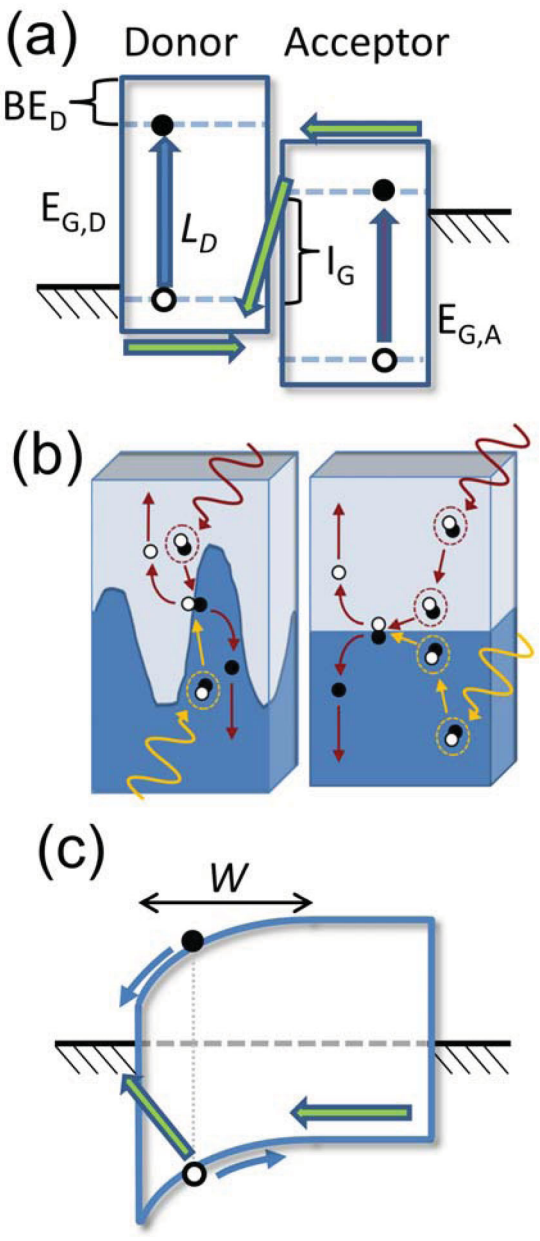

Figure 4. Illustration of the energy diagram for a) a donor–acceptor heterojunction under short-circuit conditions (fully depleted) where the V_{OC}-limiting recombination current is highlighted by green arrows and b) a bulk-heterojunction architectures utilized in small-molecule, organic, and polymer cells. c) Energy diagram for a Schottky junction under short-circuit condition. $E_{G,D}$ and $E_{G,A}$ are the optical gap of the donor and acceptor, respectively; BE_D is the exciton binding energy in the donor, L_D is the exciton diffusion length, and I_G is the donor–acceptor interface gap for recombination.

L_D) to the exciton-dissociating bilayer interfaces. As thicker layers are needed to absorb more light and thinner layers are desired to facilitate excitons reaching dissociative bilayer interfaces, the tradeoff requires optimization of the nano-PV layer thickness for the maximized device performance. The *EQE* can therefore be described in terms of the constituent efficiencies as $EQE = \eta_A \eta_{ED} \eta_{CT} \eta_{CC}$ where η_A is the absorption efficiency, η_{ED} is the exciton diffusion efficiency, η_{CT} is the charge-transfer or dissociation efficiency, and η_{CC} is the charge collection efficiency. In the absence of optical interference, $\eta_A = T(1 - \exp(-\alpha d))$ where T is the total transmission through the substrate and the transparent conductive oxide electrode to the active layer (typically limited to at most 75%), α is the absorption coefficient, and d is the active layer thickness; $\eta_{ED} = \exp(-d/L_D)$; $\eta_{CT} \approx 1$ for a large donor–acceptor energy offset that drives efficient exciton dissociation at the bilayer interface; $\eta_{CC} = L_C/d(1 - \exp(-d/L_C))$, where L_C is the charge collection length.[20,21] This model for the *EQE* is plotted in **Figure 5** as a function of αd for various values of αL_D and αL_C. Typical values for αL_D are ≤ 1 so that for planar PV structures, exciton diffusion is the limiting process.[3]

Bulk-heterojunction (BHJ) structures aim to decouple these two limiting efficiencies through the use of interpenetrating networks of donor and acceptor (shown schematically in Figure 4b), which enable the surface area of the dissociating interface to be dramatically increased. This effect manifests as an effective enhancement of L_D which, in turn, enables the optimal device thickness to be increased as shown in Figure 5. However, as the interpenetration of the donor–acceptor network increases the pathways for charge collection become hindered, which is also a common limitation even in planar structures where αL_C can be <1. Indeed the mobility (μ) of organic semiconductors is generally quite low, in the range of 10^{-7} cm^2 V^{-1} s^{-1}) to 10 cm^2 V^{-1} s^{-1}.[22] Thus, there is a sensitive interplay between high photocurrent generation and charge collection that requires careful morphology optimization. While solid state BHJ structures typically suffer from the hindered carrier transport, they nonetheless remain the highest-performing solid-state nano-PV cells to date. Alternative approaches to simultaneously increase η_{ED} and η_{CC} include 1) long-range ordering which can effectively increase both L_D[23–25] and charge mobility[22] or 2) molecular design of highly absorptive materials (with high values of α) or effective light trapping schemes to reduce the required thicknesses while maintaining high absorption efficiency.[26]

The energy-level offset at the bilayer junction interface impacts the open-circuit voltage. For such donor–acceptor organic cells, the maximum V_{OC} has been shown in several studies to be proportional to the "interface gap" as outlined in Figure 4, where the dark current is limited through charge recombination at the heterojunction interface due the energy-level offset at the junction.[27,28] Non-optimized electrode work functions can further reduce V_{OC} from this maximum by creating charge collection barriers that can result in a build-up of space charge.[29] For ohmic contacts, the maximum V_{OC} for bilayer organic cells can be expressed as[28]

$$V_{OC}^{Max} \leq E_A^{LUMO} - E_D^{HOMO} - \Delta E_{BE} \quad (7)$$

where E_A^{LUMO} is the acceptor lowest unoccupied molecular orbital (LUMO) energy, E_D^{HOMO} is the donor highest occupied molecular orbital (HOMO) energy, and ΔE_{BE} is the interface charge-transfer (CT) state binding energy. With optimized donor–acceptor energy levels, the interface gap is still ultimately constrained by the smaller of the optical gaps minus the binding energy. Accordingly, organic heterojunctions exhibit a wide range of photovoltages for various donor/acceptor combinations with similar optical gaps, as shown in Figure 1. For

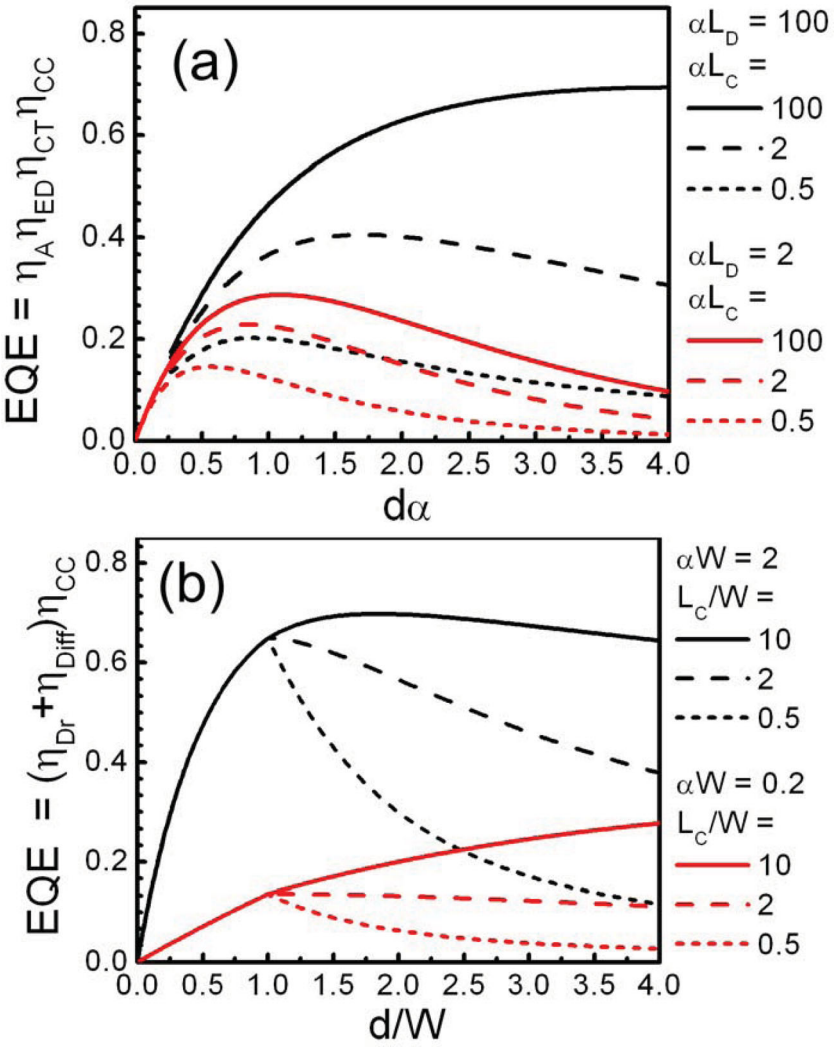

Figure 5. a) Calculation of the *EQE* in the absence of singlet fission for donor–acceptor heterojunction as a function of the exciton diffusion length, L_D, absorption coefficient, α, and carrier diffusion length L_C highlighting the exciton diffusion bottleneck. For the absorption efficiency (η_A) the transmission to the active layers is taken as T = 75%, limiting the maximum *EQE*. b) Calculated *EQE* for Schottky diodes (or p–n junctions with optical transparent p (or n) region) in the absense of multiexciton generation as a function of depletion width W, absorption coefficient, α, and carrier diffusion length, L_C.

the surveyed nano-PVs we find the photovoltage constrained to 80% of the SQ voltage, which is roughly equivalent to replacing E_G in Equation 5 with $E_G - \Delta E_{BE}$ and fitting the heuristic of $\Delta E_{BE} \approx 0.17 E_G$. Although polymer solar cells are similarly limited in photovoltage by Equation 7, reduction of this loss has recently led to V_{OC}'s surpassing those of other nano-PV technologies.[30–32]

Certified power conversion efficiencies reaching 6% to 8% have already been reported for both vapor-deposited small molecule and polymer solution-processed cells with spectral responsivities from λ = 350 nm to λ = 800 nm.[33–37] Future improvements will need to focus on maintaining low interface recombination (i.e., through interface engineering), extending absorption deeper into the infrared while simultaneously maintaining the high photocurrents and charge collection efficiencies already achieved in the best devices. Accordingly, this will require a combination of morphology optimization and material engineering of molecules with long diffusion length, high carrier mobilities, and smaller bandgaps. Indeed, engineering optical gaps in organic molecules into the infrared remains a significant challenge, one that may be overcome through the use of hybrid material systems such as organic/colloidal-quantum-dot or organic/nanotube[38,39] combinations. Stacked structures in which each stacked cell can be optimized for a different wavelength range may also be key to enabling efficient harvesting of light at longer wavelengths.[3,36,40,41]

4.2. Dye-Sensitized Solar Cells (DSSC)

High efficiency, DSSC cells with certified η_p = 11% have been demonstrated utilizing Ru-based organic dyes with absorption from the UV to λ = 800 nm (Figure 1,2).[34,42] These high power conversion efficiencies are largely attributable to near unity internal quantum efficiencies (*IQE*) and fill factors around 70%. DSSCs are a form of organic BHJ structure that have demonstrated nearly complete decoupling of exciton diffusion and absorption efficiency through the formation of an intercalated dissociating interface between a monolayer of dye molecules and a nanostructured acceptor layer. The high fill-factors stem from the replacement of molecular acceptors with a high electron-mobility inorganic semiconductor, typically a sintered mesoporous TiO_2, along with a highly conductive liquid electrolyte to efficiently extract charges. Although little advance has been made in terms of increasing η_P since the early reports, a number of different dye systems have approached this high level of performance (Figure 2).[43–45] Recent reviews of DSSC PVs can be found in ref. [13] and [46]. Exploring the divergence of the demonstrated DSSC power conversion efficiencies from the calculated limits indicates that the shortfall in efficiency is mostly due to the low photovoltage. This low V_{OC} likely results from a combination of direct charge recombination from the TiO_2 to the triiodide redox mediator and the low conduction band energy of TiO_2, or low interface gap, where Equation 7 is directly applicable to DSSC cells. Indeed, the observed V_{OC} values remain significantly lower than other organic–polymer cells of similar bandgap.

Operational stability may also be an issue in liquid-phase DSSC due to the volatile electrolyte. Recent efforts have therefore focused on the development of solid-state hole transport layers (HTL), with record efficiencies for these devices of around 5–6%.[47–52] In several of these cases direct substitution

of the tri-iodide electrolyte solution for a solid state HTL typically reduced the efficiency by approximately two-fold due to reduction in the *FF* and J_{SC} and is suggestive of a need for higher mobility solid state HTLs in both DSSC and OPV structures. Again, tailoring organic dyes with absorption into the near-infrared (with1.1 eV bandgap) remains a challenge for improving DSSC efficiencies as well. Alternatively, DSSC devices with colloidal quantum dot light absorption centers with near infrared bandgaps could be viable in generating higher V_{OC}.[51,53–55]

4.3. Colloidal Quantum Dot PVs

CQDs are hybrid materials composed of nanocrystal cores of inorganic semiconductors, capped with (typically) organic ligands. The distinguishing feature of colloidal quantum dots is the finite nanocrystal size that leads to electronic confinement, tunable band structure, and improved processability as compared to their bulk semiconductor counterparts. CQDs, compared to most small molecule and polymer semiconductors, exhibit very large effective dielectric constants. For example[56,57] ε_{PbS} = 15–20 (bulk PbS[58] = 170) and ε_{PbSe} = 12–50 (bulk PbSe[58] = 210) for ethylene-dithiol-capped PbS CQD. These large bulk dielectric constants lead to large effective Bohr radii (of between 10 and 20 nm) and hence make quantum confinement effects important in particles of this size. Confinement can impact the optical gap[59] which can be tuned over a range of meV to eV, providing a method to move through E_G-space in Figure 1,2. The exciton binding energy, which is proportional[60] to $1/\varepsilon^2$, is therefore small ($<kT$), indicating that free-carrier and field-driven dissociation are typically dominant, at least within individual CQDs.[61] Therefore, in contrast to molecular, polymeric, and DSSC PVs, the CQD PVs do not require a heterojunction for carrier dissociation, but rather excitons can dissociate within the CQD thin film bulk. Solution-deposited CQD Schottky diodes have recently been constructed with benzenediothiol (BDT)-capped-PbS CQDs exhibiting $\eta_P \approx 4\%$ and internal quantum efficiencies approaching 80%.[62] Metal oxide/PbS-CQD n–p junctions have also been reported with η_P = 5.7%[63] and >1000 hour lifetime.[64]

Without the bottleneck of exciton diffusion, CQD PVs are limited only by low light absorption efficiencies, low charge carrier mobility, and depletion widths that limit the optimal film thickness. The charge transport through CQD films is similar to organic semiconductors in that various forms of variable-range carrier hopping have been observed,[57] while charge carrier mobilities are similar in magnitude to the amorphous and crystalline organic layers.[65,66]

For Schottky diodes (or p–n junctions with an optically transparent wide-bandgap p-region) with CQD layer thickness of *d*, the external quantum efficiency is a function of both the efficiency of current generation in the depleted (η_{Dr}) and quasineutral regions (η_{Diff}) of the CQD film, where $EQE = (\eta_{Dr}\,\eta_{CT} + \eta_{Diff}\,\eta_{CT})\eta_{CC}$. For $d < W$ (where W is the width of the charge depletion region), $\eta_{Diff} = 0$, $\eta_{CC} = 1$ due to drift collection, and $\eta_{Dr} = T(1 - \exp(-\alpha d))$ where η_{CT} is the field-dependent charge dissociation efficiency, assumed to be 1 due to the small exciton binding energy. For $d > W$, $\eta_{Dr} = T(1 - \exp(-\alpha W))$, $\eta_{Diff} = T(1 - \exp(-\alpha(d - W)))\exp(-\alpha W)$, and the charge collection through the diffusion region[20,21] is $\eta_{CC} \approx \frac{L_C}{d-W}\left(1 - \exp\left(-\frac{d-W}{L_C}\right)\right)$. The *EQE* is plotted in Figure 5b as a function of d/W for various values of αW and L_C/W. Photocurrent is primarily generated in the depletion region of width, *W*, where exciton dissociation and carrier drift are aided by the built-in potential. For large carrier collection efficiencies, current can also be contributed from the quasineutral region. Therefore, finding techniques to increase the carrier mobility of these films, for example by employing inorganic ligands,[67] decreasing inter-CQD spacing,[68] or employing superlattice ordering of CQDs,[61] could lead to larger optimal devices thicknesses and a near doubling of photocurrents over devices at the present state of the art. The near-IR response of CQD solar cells is currently limited by low absorption coefficients and low optimum thicknesses of the CQD layers. Additionally, the ability to control the doping levels[69] and tune the effective dielectric constants in capped CQDs via ligand control can lead to enhanced depletion widths, which has already been shown to be critical in controlling the performance of CQD devices.[68]

5. Ultimate Performance of the Third-Generation PV Concepts

A number of architectures have been proposed for reducing losses in solar cells in order to overcome the SQ single-junction limit. These include hot carrier solar cells,[13,70] intermediate band solar cells,[13,71] up- and down-converters,[72] and concentrators,[13,73] as well as cells that utilize multiple-exciton generation,[6,74] exciton fission,[6,74] and tandem stacking.[11,13] While all of these approaches hold promise, this review focuses on the latter three, in which nanostructured materials are particularly relevant.

5.1. Multiple Exciton Generation in PVs

One approach for overcoming the SQ single-junction limit in CQD systems is through the use of multiple exciton generation (MEG). The MEG process is shown in Figure 3 whereby multiple carriers are generated from one hot-excited state. In quantum confined materials, it is suggested that the increased discretization of energy levels should lead to reduced carrier cooling rates, allowing MEG to become competitive with carrier relaxation.[59] MEG efficiency limits have recently been reviewed by Nozik, where theoretical maximum efficiencies with MEG ("infinite staircase") in the SQ limit were calculated to be η_P = 44%, significantly exceeding the η_P = 33% of the single-junction limit.[74] The onset threshold for ideal MEG occurs at nE_G, where is n is an integer multiplication number. Under AM1.5 illumination, PVs enhanced by the MEG process can add substantial additional photocurrent only when the PV photoactive layer has $E_G < 1.5$eV. This can be seen in Figure 1,2 where we calculate the practical efficiency limit for the idealized "two-staircase" MEG (labeled "M2 MEG") and show that the practical efficiency limit increases from 17.1% for the single junction cell with no MEG to 21.8% for PVs enhanced by M2 MEG. To date, no PV efficiency improvements resulting in *EQE* > 100% have been

reported, hence the benefit of the MEG enhancement in PVs has not yet been demonstrated. As the measurements of MEG processes are still evolving, we can assess the practical benefit of implementing the MEG process in PVs by comparing it to equivalent processes that have been extensively studied such as the impact ionization (or the reverse of the Auger recombination process), which to date has been demonstrated to be only weakly present in most bulk inorganic semiconductors.[75] Likewise, recent measurements show that the overall magnitude of MEG in CQD films is also limited, with onset thresholds and multiplication-profiles that are far from ideal[59,76–79] or overestimated due to charging effects.[80,81] Calculations show that if the MEG profile onset thresholds are less than M2 MEG, the expected achievable η_P is nearly identical to that for PV cells without MEG.[74,78] Altogether, this limits the potential for η_P enhancements through an MEG process, with the benefit of MEG enhancement of PVs only present if nearly ideal MEG process can be achieved for small gap materials.

5.2. Singlet Exciton Fission in PVs

The singlet exciton fission (SF) in organic semiconductors is a nearly equivalent analog of MEG in CQDs. In the SF process, one high energy singlet exciton at the band edge spontaneously separates to form two triplet excitons, each with ≤1/2 (singlet energy) $\pm kT$. While this process has been observed for a range of polyacene crystals,[82–85] the quantum mechanical mechanism has only recently been explored.[86] Ideal SF can result in a doubling of the photogenerated current at a given bandgap[87] and has been suggested as a method for slightly increasing multijunction PV efficiencies through improved current matching.[6,88] Moreover, it has been speculated that access to the triplet state could lead to enhanced diffusion lengths and bridge the gap between experimentally observed and theoretically predicted maximum photocurrents.[87,89] Although triplet diffusions lengths can sometimes exceed those of the singlet exciton,[24,25] triplet formation in the absence of singlet fission results in additional thermalization losses that lower the maximum efficiency below the practical limit calculated here. This is highlighted in a recent report of $IQE > 100\%$ for SF in a pentacene-C_{60} and tetracene-C_{60} bilayer architectures where overall EQE at zero bias and power efficiency still remain lower than other combinations of similar optical gap.[87,90]

The triplet states have negligible oscillator strength (even smaller than the MEG process) and there are rarely other optically absorptive states between the lowest singlet and triplet levels. Therefore, for our analysis $E_G = E_S$ is used as the optical gap in Equation 3 to determine the photocurrent resulting from the absorbed incident light, while $E_G = E_T = 1/2E_S$ is used in Equation 5 to determine the carrier level or V_{OC} for spontaneous fission. In Figure 1,2 we refer to this case as "SF1". We note that while the ideal MEG process in CQD films acts similarly to stacking tandem PV cells (as discussed below), singlet fission in a single organic thin film layer does not. In the SF1 case the maximum achievable η_P is lower than for the single junction cells that do not exhibit singlet fission because the decrease in the open circuit voltage is more severe than the gain in the photocurrent (Figure 1). If the V_{OC} scaled exactly as E_G (i.e., without an offset) as assumed by Beard and Nozik, then the efficiency limit would be unchanged from the M1 case.[91]

An alternative device configuration utilizing SF in a PV is with a donor-acceptor pair consisting of an SF material with large bandgap that forms a junction with a non-SF material whose gap is half as large (vis, same as the triplet gap). This case, which we refer to as "SF2" in Figure 1,2, results in the same maximum η_P as the M2 MEG case. Additionally, this approach would require structured absorption in the low-gap material so that higher energy photons are preferentially absorbed only within the SF layer and not thermalized in the non-SF layer. The SF2 pairing would therefore be less compatible with BHJ and DSSC architectures[90,92] where such optical engineering becomes more challenging and would result in thermal losses approaching the M1 scenario. Figure 3 outlines both SF1 and SF2 schemes.

5.3. Tandem PVs

The tried method for simultaneously reducing thermalization and absorption losses is to stack multiple cells with varying bandgaps, so that each cell absorbs a different part of the solar spectrum. Indeed, this approach has led to record PV efficiencies of 42.3% with GaInP/GaInAs/Ge two-terminal, triple junction cells.[2] While tandem stacking of high efficiency inorganic cells is limited by epitaxial growth considerations (i.e., lattice matching) and can add substantial cost to PV fabrication, nanostructured materials do not have such restrictions. This makes tandem growth of nano-PVs feasible on arbitrary substrates and with arbitrary combinations of subcells, as already demonstrated for molecular PV structures.[93]

Tandem stacking of multiple cells requires matching the photocurrents (for series connection) or photovoltages (for parallel connection) of the stacked subcells (i.e., matching maximum power points). Series matching generally leads to higher efficiencies since cells in parallel are limited by the voltage of the lowest gap cell.[72] However, parallel tandem junctions can also exhibit better light-shading stability where the photovoltage is logarithmic with light intensity and therefore could be useful under highly variable illumination conditions.[94] Therefore, in contrast to the MEG and SF approaches, excess thermal energy in tandem structures can be utilized to build either current (in parallel integration) or voltage (in series stacking). Utilizing the assumptions of SQ, the maximum efficiency for series two-cell, three-cell, and infinite number of tandem cells are 43%, 48%, and 67%, respectively.[74] However, assuming a non-idealized PV performance (discussed before for the M1 case in Figure 2), we calculate a maximum practical laboratory power conversion efficiency of 24% for a stacked, current-matched, two-cell nano-PV tandem structure (compared to the predicted 43.4% in the SQ limit). This performance is slightly better than the maximum η_P for M2 MEG or SF2.

While tandem architectures for small-molecule and polymer PVs have been demonstrated, full optimization of such structures will require subcells with responsivity deeper into the near IR (NIR). Accordingly, tandem PVs could be designed from a combination of CQD and organic containing subcells, where the infrared responsivity of CQD layers can complement

the visible spectrum response of organic layers, provided that future CQD subcells can be optimized for complete NIR absorption. We also note that tandem stacking of two or more identical PV cells (cells with the same E_G) can help in overcoming deleterious effects of series resistance that reduce *FF*.[95] For a given light absorption, such a stacked geometry would reduce the active layer thicknesses of individual subcells, which would diminish exciton diffusion and charge collection losses, particularly for CQD devices with fixed depletion widths or organic materials with fixed exciton diffusion lengths.[36,96,97]

6. Projected Cost of Nano-PV Technologies

As the efficiencies of nanostructured solar cells advance toward the limits discussed above, the critical determinant of their commercial viability will be the levelized energy cost (LEC) of electricity they produce, in \$ kW^{-1} h^{-1}, relative to the incumbent means of energy production including electricity from fossil fuel power plants and from other PV technologies. The LEC is a suitable metric because it can readily be compared to the present-day costs of coal and gas-generated electricity. It also accounts for variable module lifetime, to be discussed in detail in the next section, as well as the balance of systems (BOS) costs.[98]

Presently, the PV contribution to USA electricity generation is less than 0.2%.[99] If the USA PV deployment continues to rise at the recently seen[100] 40% year-to-year growth rate, it would take 15 years for PV technologies to account for 20% of USA electricity production (note that at a slower, but still high, year-to-year growth rate of 25%, it would take over 20 years to reach 20% of USA electricity production). We set 20% as a target PV penetration in USA electricity production, since for the foreseeable future, inputs into the USA electrical grid from intermittent renewable energy sources, such as PVs, are expected to be limited to between 10% and 20% due to issues of grid stability.[101] Advancements of energy storage and "smart-grid" technologies would increase the allowable fraction of intermittent power sources on the electrical grid. Therefore, we expect that in the next two decades PV technology can aim to displace at most 20% of the non-renewable energy generation, with the biggest economic benefit provided when displacing the presently most expensive electrical energy. To estimate the LEC cost targets that need to be met, we plot in **Figure 6** the cost of USA electricity across all sectors (residential, commercial, and industrial) integrated over kW h consumed.[102] The 20% of the most expensive electricity consumed in the USA cost more than \$0.12 kW^{-1} h^{-1}, setting this as a near-term target of the cost-competitive LEC for the nano-PV generated electricity. LEC of approximately \$0.05 kW^{-1} h^{-1} would be needed to compete with all modes of electricity generation across all sectors. We note that subsidies for oil and fossil fuel-based energy have been estimated to outnumber those for renewable sources of energy by roughly a factor of three.[103] A reversal in this trend could substantially shift the LEC competition point in a direction favorable for PV technologies.

To assess LEC sensitivity to lifetime, efficiency, and module cost, we estimate the LEC according to:[104,105]

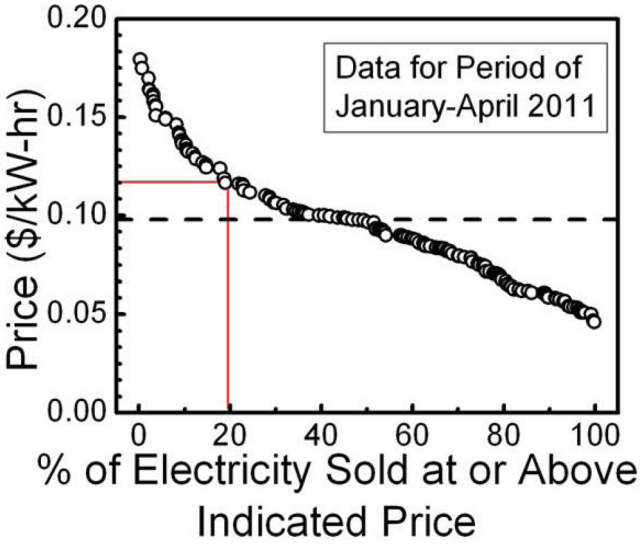

Figure 6. Estimate of the fraction of electrical energy paid in the USA at or above a given price; data adapted from ref. [102]. The average end-use price is highlighted by the dashed line and the price point to fill the costliest 20% of USA electricity is highlighted by solid red lines.

$$LEC = \frac{ICC1000CRF}{CF8760} + O\&M \tag{8}$$

ICC is the installed capital cost (\$ W_P^{-1}) (where W_P refers to the watts of power generated under peak illumination conditions), defined as the sum of the module and BOS costs (\$ m^{-2}) divided by power (W m^{-2}) produced; *CF* is the capacity factor, which takes into account considerations such as diurnal and seasonal variation in insolation, assumed to be 15.5% (e.g., Kansas City);[105,106] O&M are operations and maintenance costs, assumed to be 0.001 \$ kW^{-1} h^{-1}.[104,107] Finally, CRF is the capital recovery factor:

$$CRF = \frac{i(i+1)^n}{i(i+1)^n - 1} \tag{9}$$

The interest rate (i) is assumed to be either 6% or 10% and n is the useful operating lifetime of the PV module system.

For reference, the module costs of OPV and DSSC modules have been previously estimated to be in the range of 20 to 40 \$ m^{-2} and 45 to 120 \$ m^{-2}, respectively.[106] BOS costs have been estimated for several types of module installation including ground-mounted systems (40 to 90 \$ m^{-2}), commercial rooftop mounting with glass substrates/superstrates (75 to 135 \$ m^{-2}), and rooftop systems with modules based on flexible laminates (54 to 99 \$ m^{-2}).[106,107] These figures are based on the assumption that best practices for manufacturing and installation are similar to those of other thin film PV technologies (e.g., CdTe, copper indium gallium (di)selenide (CIGS), amorphous(a)-Si).[108]

In **Figure 7**a we consider a conservative scenario in which the nano-PV module cost is 75 \$ m^{-2} and the rooftop-mounted BOS cost is also 75 \$ m^{-2}. The LEC is calculated for such modules with lifetimes ranging from 5 to 20 years and with power conversion efficiency ranging from 5% to 25%. Additionally, we

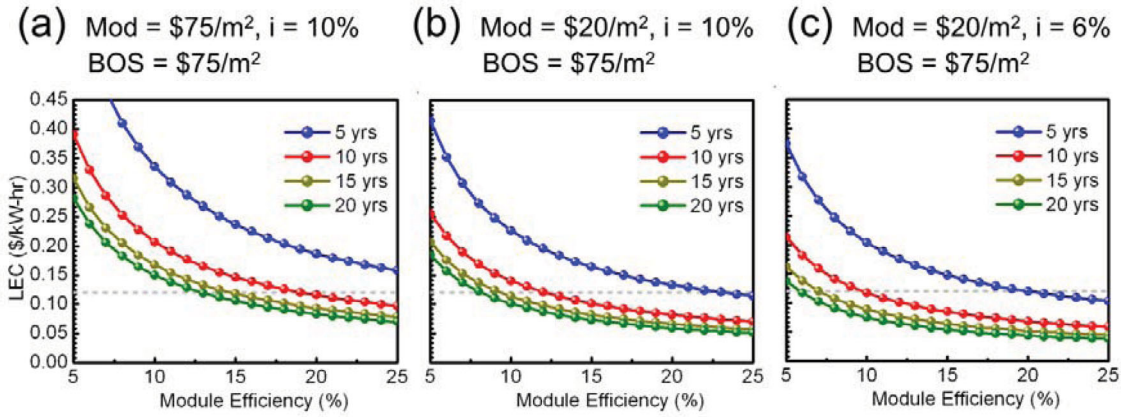

Figure 7. Estimated levelized energy cost ($ kW^{-1} h^{-1}) as a function of both module efficiency and lifetime for various cost scenarios: a) Scenario of an intermediate BOS cost (75 $ m^{-2}) (estimated for rooftop mounting) and a conservative module cost (75 $ m^{-2}). b) Scenario of lower-limit module cost (20 $ m^{-2}). c) Best-case scenario with lower-limit module costs and also a reduced financing rate (i = 6%). Note that a laboratory efficiency has to be scaled by roughly 0.75 to estimate the losses in scaling to a module efficiency.

consider in Figure 7b the impact of realizing the full low-cost potential of nano-PV by calculating the LEC assuming the lowest estimated module cost of 20 $ m^{-2}. Finally, Figure 7c shows the same calculations from Figure 7b, but with the interest rate lowered from i = 10% to i = 6% (the best-case cost scenario).

For each of the plots in Figure 7 we find that the LEC flattens out as the module efficiency or lifetime increases suggesting that the steepest gains in LEC occur with improvements of relatively low module efficiencies and lifetimes. For the most conservative assumptions of module and BOS cost utilized (Figure 7a), modules with lifetimes $n \geq 15$ years and $\eta_P \geq 15\%$ result in the cost-competitive LEC ≤ 0.12 $ kW^{-1} h^{-1}, enabling their market penetration. By lowering the module cost from 75 $ m^{-2} to 20 $ m^{-2} (as in Figure 7b), nano-PVs can reach cost-competitive LEC with a 10 year lifetime and $\eta_P \geq 12\%$, a power conversion efficiency achievable within the practical efficiency limits estimated above. Reduction in the financing interest (as in Figure 7c) would further reduce the requirements for nano-PVs with cost-competitive LEC to $\eta_P \geq 10\%$ and 10 year lifetime. In this case, if nano-PV modules are realized close to our estimated practical efficiency limits and with lifetimes of between 10 and 20 years, LECs for M1 single and two-junction tandem cells of between 0.10 and 0.06 $ kW^{-1} h^{-1} and between 0.07 and 0.04 $ kW^{-1} h^{-1} are possible, respectively (we take the practical laboratory efficiency limits of 17% and 24% for single- and tandem-junction cells, respectively, and multiple by 0.75 to estimate the practical module efficiency limits).[109] Thus, the degree of market penetration will be highly dependent on the ability to fully realize the low-cost manufacturing of nano-PVs as well as advances in both efficiency and cell lifetime.

Manufacturing cost structures required to reach these LECs may be enabled by processing active layers with low-temperature vapor-phase or solution processing techniques, often employed in the fabrication of nano-PVs. While the ultimate and relative cost advantages of these two processing techniques remain unclear, the ability to process active layers at low temperatures and onto inexpensive flexible substrates should enable a reduction in the manufacturing as well as infrastructure costs. For example, flexible and light-weight PV modules will likely have a greater amenability to integration with existing infrastructure (building-integrated photovoltaics), which could significantly reduce the amount of dedicated framing/support required for installation. Such optimization and integration is expected to substantially lower BOS costs.[107,110]

7. Operating Lifetime of Nano PVs

The inherently nanostructured forms of DSSCs, molecular and polymeric organic PVs (OPVs), and CQD PVs can lead to instabilities in their operation under thermal and optical stress, which do not affect conventional monolithic inorganic PVs. For example, DSSCs could suffer electrolyte leakage under thermal expansion and bleaching or desorption of the photopactive dye;[111] OPVs could undergo morphological change to the active layer and photo-oxidation under environmental exposure;[112,113] and CQD PVs are often subject to loss of ligands that passivate the QD surface and can undergo rapid oxidation of the semiconductor shell/core.[114] Additional degradation mechanisms include indium diffusion from the indium tin oxide (ITO) electrode[115] and delamination or oxidation of the low-work-function cathode.[116] Nonetheless, some of these challenges have already been overcome in the similar field of organic light-emitting diodes, where long lifetimes (>10 years)[117,118] have been demonstrated and commercialization is well underway.

Plots in Figure 7 shows us that in an assessment of a nano-PV technology in terms of $ kW^{-1} h^{-1}, the useful lifetime of the device, typically reported as T_{80} (the time for the device to decay to 80% of its initial performance under standard operating conditions), is as important as the initial efficiency. Standardized conditions and procedures for lifetime testing are thus necessary for the effective comparison of different device architectures and encapsulation methods. A frequently employed accelerated lifetime testing method consists of a 1000 hour light soak under constant AM1.5G illumination (100 mW cm^{-2}) and elevated temperature (50–60 °C) with continual monitoring of the photovoltaic operational parameters (J_{SC}, V_{OC}, FF, and PCE).[111,119] This submits the device to roughly the same

number of optical excitations experienced during ≈0.5 years of outdoor operation in North America, where the annual mean level of irradiance is ≈5 kW hr m^{-2} d.[107] A representative collection of 1000-hour lifetime testing results for various nano-PV architectures is compiled in **Table 2**.

It should be noted that nano-PVs rarely undergo a simple linear decay[120] in the efficiency with time, but are often characterized by a "burn-in" period involving a relatively rapid increase or decay of the initial performance, followed by a period of slow, linear decay.[119,121] Because of O_2 and H_2O sensitivity[120] of many of the active layers to degradation, packaging technology will be crucial.[121] Accordingly, catastrophic failures in packaging may also rapidly degrade the performance at any point during the test. Given the unpredictable nature of device degradation, extended lifetime tests under conditions approximating those expected under normal operation, either in an outdoor environment or under repeated illumination and heating cycles, are particularly relevant. A sample of extended lifetime testing results for DSSCs and OPVs is compiled in **Table 3** and indicates that, with effective encapsulation strategies, the lifetime of these nanostructured PVs can be relatively long. Toyoda et al. report a relative degradation of only 16% for a DSSC after 2.5 years of outdoor testing,[122] and Pfeiffer et al. observe no significant degradation of a 6% tandem OPV after 5000 hours of constant 1.5 sun illumination under open-circuit conditions.[95] Ultimately, addressing lifetime and efficiency simultaneously will be critical in determining the adequacy of nano-PV technologies for electricity production. Device efficiency and lifetime are not necessarily independent. Sensitivity to UV photons, for instance, may contribute to a slightly higher initial PV cell efficiency, but at the expense of a faster cell degradation.

Table 2. 1000 hour constant-illumination nanostructured PV testing.

Active material	Device architecture	Initial η_p [%]	After 1000 h light soak [% of initial]	Temperature [°C]	Ref.
DSSC					
Z907	Polymer gel electrode	6.1	96	55	[169]
K77	Nonvolatile electrode	9	99	60	[170]
C103	Ionic liquid electrode	8.5	94	60	[171]
CYC-B11	Low-volatility liquid electrode	8.2	93	60	[172]
C217 (Ru-free)	Ionic liquid electrode	8.1	96	60	[173]
OPV					
P3HT:PCBM	BHJ (flexible)	3	85	65	[174]
ZnPc:C_{60}	Planar heterojunction	2.8	84	50	[175]
ZnPc:C_{60}	Tandem (same subcells)	4.1	100	50	[95]
QDPV					
PbS	ZnO/PbS np heterojunction	3	95	20	[64]

Table 3. Extended nanostructured PV lifetime testing.

Material	Device architecture	Initial η_p [%]	Duration [h]	Condition	After test [% of initial]	Ref.
DSSC						
N719	Ionic liquid electrode	–	22000	Outdoors	84	[122]
OPV						
P3HT:PCBM	Polymer BHJ	1	10000	Outdoors	103	[176]
P3HT:PCBM	Polymer BHJ	4.0	4400	Light soak	74	[121]
PCDTBT:PCBM	Polymer BHJ	5.5	4400	Light soak	69	[121]
Undisclosed	Small-molecule BHJ (tandem)	6.07	5000	Light soak	100	[36]

Table 4. CO_2 emission factors (EF) for organic photovoltaic modules. Data adapted from ref. [36] where the embodied CO_2 and energy input from module production is estimated to be 110 kg m^{-2} and 2800 MJ m^{-2}, respectively, and the average irradiance is taken to be 5 kW h m^{-2} d.

Module efficiency	Lifetime [yr]	Generated power [kW h]	CO_2 EF [g CO_2 kW^{-1} h^{-1}]
5%	5	340	330
5%	10	680	165
10%	10	1360	83
13%	20	3536	32
18%	20	4896	23
European Wall (2006)	–	–	411

Beyond commercial viability, PV cell lifetime is acute in the lifecycle analysis and carbon footprint. To have any impact on reducing carbon emission, solar cells require lifetimes longer than the energy payback time; since the present PV cells will be produced by using electricity that is primarily generated through burning of the fossil fuels, the CO_2 emission factor of PVs is then inversely proportional to the cell lifetime and efficiency. For example, one recent study calcuated that the energy payback time is 4 and 2 years for a 5% and 10% OPV, respectively.[123] For a lifetime of 15 years, the carbon emission factors for 5% and 10% efficient modules are 110 and 55 kg CO_2 kW_P^{-1}, respectively, which compares favorably to, for example, the average 2006 European electricity CO_2 emission factor of 400 kg CO_2 kW^{-1} (**Table 4**).[123,124] A reduction in the lifetime to 5 years would significantly diminish the carbon footprint advantage of nano-PVs, particularly if η_P remain below 10%. While the cell lifetime has only a small impact on overall cost for $n > 10$ years (Figure 7), extending lifetimes well beyond this range will have a significant role in the ability to produce and promote "clean" renewable energy. Nonetheless, with widespread adoption of solar and other renewable energy generation, carbon emission factors in PV production can be further reduced to approach near-zero carbon footprints.

8. Conclusions

We have reviewed the limits to the performance of molecular, organic, polymeric, dye-sensitized, and CQD-based solar cells.

We have considered the specific challenges associated with improving the power conversion efficiency of each and analyzed benefits of several approaches for reduced thermal losses beyond the single bandgap limit. Critical considerations related to the module lifetime and cost that are unique to nano-PV architectures have been quantified. While there may be substantial niche markets for low-cost and low-efficiency PV (i.e., point of source PV utilization), the scaling required to have a significant impact on energy markets will most likely be achieved through PV systems for grid power generation. Our analysis suggests that a practical single-junction laboratory PCE limit of 17% and a two-cell tandem PCE of 24% are achievable. When combined with operating lifetimes of 10 to 15 years, such performance could indeed position nano-PV cells as a transformational technology for solar energy markets.

Acknowledgements

T.P.O. and P.R.B. contributed equally to this work. This work was supported by Eni S.p.A. under the Eni-MIT Alliance Solar Frontiers Program. The authors thank Tonio Buonassisi and William Tisdale for insightful discussions. T.P.O. gratefully acknowledges support from the National Science Foundation Graduate Research Fellowship Program and the Link Foundation. P.R.B. is generously supported by the Fannie and John Hertz Foundation Fellowship and J.A.R. is generously supported by the National Science Foundation Graduate Research Fellowship Program.

Received: September 4, 2011
Published online:

[1] M. I. Hoffert, K. Caldeira, G. Benford, D. R. Criswell, C. Green, H. Herzog, A. K. Jain, H. S. Kheshgi, K. S. Lackner, J. S. Lewis, H. D. Lightfoot, W. Manheimer, J. C. Mankins, M. E. Mauel, L. J. Perkins, M. E. Schlesinger, T. Volk, T. M. L. Wigley, *Science* **2002**, *298*, 981.
[2] M. A. Green, K. Emery, Y. Hishikawa, W. Warta, *Prog. Photovoltaics* **2011**, *19*, 84.
[3] S. R. Forrest, *MRS Bull.* **2005**, *30*, 28.
[4] C. J. Brabec, N. S. Sariciftci, J. C. Hummelen, *Adv. Funct. Mater.* **2001**, *11*, 15.
[5] M. A. Green, *Prog. Photovoltaics* **2001**, *9*, 123.
[6] M. C. Hanna, A. J. Nozik, *J. Appl. Phys.* **2006**, *100*, 074510.
[7] W. Shockley, H. J. Queisser, *J. Appl. Phys.* **1961**, *32*, 510.
[8] M. A. Green, *IEEE Trans. Electron Devices* **1984**, *31*, 671.
[9] T. Tiedje, E. Yablonovitch, G. D. Cody, B. G. Brooks, *IEEE Trans. Electron Devices* **1984**, *31*, 711.
[10] M. A. Green, K. Emery, Y. Hishikawa, W. Warta, *Prog. Photovoltaics* **2011**, *19*, 84.
[11] C. H. Henry, *J. Appl. Phys.* **1980**, *51*, 4494.
[12] Optical gap edge is estimated from published EQE data to be the edge of useful photocurrent.
[13] A. Luque, S. Hegedus, *Handbook of Photovoltaic Science and Engineering*, Wiley, West Sussex, England **2003**.
[14] M. D. Perez, C. Borek, S. R. Forrest, M. E. Thompson, *J. Am. Chem. Soc.* **2009**, *131*, 9281.
[15] N. C. Giebink, G. P. Wiederrecht, M. R. Wasielewski, S. R. Forrest, *Phys. Rev. B* **2011**, *83*.
[16] M. Pope, C. E. Swenberg, *Electronic Processes in Organic Crystals and Polymers*, Oxford University Press, New York **1982**.
[17] P. Peumans, S. R. Forrest, *Chem. Phys. Lett.* **2004**, *398*, 27.
[18] P. Peumans, A. Yakimov, S. R. Forrest, *J. Appl. Phys.* **2003**, *93*, 3693.
[19] C. W. Tang, *Appl. Phys. Lett.* **1986**, *48*, 183.
[20] R. S. Crandall, *J. Appl. Phys.* **1983**, *54*, 7176.
[21] J. G. Xue, B. P. Rand, S. Uchida, S. R. Forrest, *J. Appl. Phys.* **2005**, *98*, 124902.
[22] N. Karl, *Synth. Met.* **2003**, *133*, 649.
[23] R. R. Lunt, J. B. Benziger, S. R. Forrest, *Adv. Mater.* **2010**, *22*, 1233.
[24] R. R. Lunt, N. C. Giebink, A. A. Belak, J. B. Benziger, S. R. Forrest, *J. Appl. Phys.* **2009**, *105*, 053711.
[25] H. Najafov, B. Lee, Q. Zhou, L. C. Feldman, V. Podzorov, *Nat. Mater.* **2010**, *9*, 938.
[26] S. B. Rim, S. Zhao, S. R. Scully, M. D. McGehee, P. Peumans, *Appl. Phys. Lett.* **2007**, *91*.
[27] C. J. Brabec, A. Cravino, D. Meissner, N. S. Sariciftci, T. Fromherz, M. T. Rispens, L. Sanchez, J. C. Hummelen, *Adv. Funct. Mater.* **2001**, *11*, 374.
[28] B. P. Rand, D. P. Burk, S. R. Forrest, *Phys. Rev. B* **2007**, *75*, 115327.
[29] D. Rauh, A. Wagenpfahl, C. Deibel, V. Dyakonov, *Appl. Phys. Lett.* **2011**, *98*, 133301.
[30] S. Hellstrom, F. L. Zhang, O. Inganas, M. R. Andersson, *Dalton Trans.* **2009**, 10032.
[31] C. R. McNeill, A. Abrusci, J. Zaumseil, R. Wilson, M. J. McKiernan, J. H. Burroughes, J. J. M. Halls, N. C. Greenham, R. H. Friend, *Appl. Phys. Lett.* **2007**, *90*, 1293506.
[32] E. R. Wang, L. T. Hou, Z. Q. Wang, S. Hellstrom, W. Mammo, F. L. Zhang, O. Inganas, M. R. Andersson, *Org. Lett.* **2010**, *12*, 4470.
[33] H. Y. Chen, J. H. Hou, S. Q. Zhang, Y. Y. Liang, G. W. Yang, Y. Yang, L. P. Yu, Y. Wu, G. Li, *Nat. Photonics* **2009**, *3*, 649.
[34] M. A. Green, K. Emery, Y. Hishikawa, W. Warta, *Prog. Photovoltaics* **2010**, *18*, 346.
[35] S. H. Park, A. Roy, S. Beaupre, S. Cho, N. Coates, J. S. Moon, D. Moses, M. Leclerc, K. Lee, A. J. Heeger, *Nat. Photonics* **2009**, *3*, 297.
[36] C. L. Uhrich, G. Schwartz, B. Maennig, W. M. Gnehr, S. Sonntag, O. Erfurth, E. Wollrab, K. Walzer, J. Foerster, A. Weiss, O. Tsaryova, K. Leo, M. K. Riede, M. Pfeiffer, *Org. Photonics IV* **2010**, *7722*, 323.
[37] M. T. Dang, L. Hirsch, G. Wantz, *Adv. Mater.* **2011**, *23*, 3597.
[38] M. S. Arnold, J. D. Zimmerman, C. K. Renshaw, X. Xu, R. R. Lunt, C. M. Austin, S. R. Forrest, *Nano Lett.* **2009**, *9*, 3354.
[39] D. J. Bindl, M. Y. Wu, F. C. Prehn, M. S. Arnold, *Nano Lett.* **2010**, *11*, 455.
[40] D. Cheyns, B. P. Rand, P. Heremans, *Appl. Phys. Lett.* **2010**, *97*, 033301.
[41] J. Y. Kim, K. Lee, N. E. Coates, D. Moses, T. Q. Nguyen, M. Dante, A. J. Heeger, *Science* **2007**, *317*, 222.
[42] B. Oregan, M. Gratzel, *Nature* **1991**, *353*, 737.
[43] T. Bessho, E. Yoneda, J. H. Yum, M. Guglielmi, I. Tavernelli, H. Imai, U. Rothlisberger, M. K. Nazeeruddin, M. Gratzel, *J. Am. Chem. Soc.* **2009**, *131*, 5930.
[44] M. K. Nazeeruddin, P. Pechy, T. Renouard, S. M. Zakeeruddin, R. Humphry-Baker, P. Comte, P. Liska, L. Cevey, E. Costa, V. Shklover, L. Spiccia, G. B. Deacon, C. A. Bignozzi, M. Gratzel, *J. Am. Chem. Soc.* **2001**, *123*, 1613.
[45] J. H. Yum, I. Jung, C. Baik, J. Ko, M. K. Nazeeruddin, M. Gratzel, *Energy Environ. Sci.* **2009**, *2*, 100.
[46] A. Hagfeldt, G. Boschloo, L. C. Sun, L. Kloo, H. Pettersson, *Chem. Rev.* **2010**, *110*, 6595.
[47] M. K. Wang, J. Y. Liu, N. L. Cevey-Ha, S. J. Moon, P. Liska, R. Humphry-Baker, J. E. Moser, C. Gratzel, P. Wang, S. M. Zakeeruddin, M. Gratzel, *Nano Today* **2010**, *5*, 169.
[48] M. K. Wang, S. J. Moon, D. F. Zhou, F. Le Formal, N. L. Cevey-Ha, R. Humphry-Baker, C. Gratzel, P. Wang, S. M. Zakeeruddin, M. Gratzel, *Adv. Funct. Mater.* **2010**, *20*, 1821.

[49] G. K. Mor, K. Shankar, M. Paulose, O. K. Varghese, C. A. Grimes, *Appl. Phys. Lett.* **2007**, *91*, 152111.
[50] J. K. Koh, J. Kim, B. Kim, J. H. Kim, E. Kim, *Adv. Mater.* **2011**, *23*, 1641.
[51] S. J. Moon, Y. Itzhaik, J. H. Yum, S. M. Zakeeruddin, G. Hodes, M. Gratzel, *J. Phys. Chem. Lett.* **2010**, *1*, 1524.
[52] B. Liu, X. Z. Liu, W. Zhang, S. Uchida, L. P. Cai, S. Ramakrishna, *Adv. Mater.* **2010**, *22*, E150.
[53] S. Ruhle, M. Shalom, A. Zaban, *ChemPhysChem* **2010**, *11*, 2290.
[54] J. A. Chang, J. H. Rhee, S. H. Im, Y. H. Lee, H. J. Kim, S. I. Seok, M. K. Nazeeruddin, M. Gratzel, *Nano Lett.* **2010**, *10*, 2609.
[55] I. Mora-Sero, J. Bisquert, *J. Phys. Chem. Lett.* **2010**, *1*, 3046.
[56] J. Tang, L. Brzozowski, D. A. R. Barkhouse, X. H. Wang, R. Debnath, R. Wolowiec, E. Palmiano, L. Levina, A. G. Pattantyus-Abraham, D. Jamakosmanovic, E. H. Sargent, *ACS Nano* **2010**, *4*, 869.
[57] J. A. Tang, E. H. Sargent, *Adv. Mater.* **2011**, *23*, 12.
[58] O. Madelung, *Semiconductors: Data Handbook*, Springer, New York **2004.**
[59] A. J. Nozik, M. C. Beard, J. M. Luther, M. Law, R. J. Ellingson, J. C. Johnson, *Chem. Rev.* **2010**, *110*, 6873.
[60] J. Kalinowski, *Organic Light-Emitting Diodes: Principles, Characteristics, and Processes*, Marcel Dekker, New York **2005**.
[61] J. J. Choi, J. Luria, B. R. Hyun, A. C. Bartnik, L. F. Sun, Y. F. Lim, J. A. Marohn, F. W. Wise, T. Hanrath, *Nano Lett.* **2010**, *10*, 1805.
[62] K. Szendrei, W. Gomulya, M. Yarema, W. Heiss, M. A. Loi, *Appl. Phys. Lett.* **2010**, *97*, 203501.
[63] H. Liu, J. Tang, I. J. Kramer, R. Debnath, G. I. Koleilat, X. Wang, A. Fisher, R. Li, L. Brzozowski, L. Levina, E. H. Sargent, *Adv. Mater.* **2011**, *23*, 3832.
[64] J. M. Luther, J. B. Gao, M. T. Lloyd, O. E. Semonin, M. C. Beard, A. J. Nozik, *Adv. Mater.* **2010**, *22*, 3704.
[65] D. A. R. Barkhouse, A. G. Pattantyus-Abraham, L. Levina, E. H. Sargent, *ACS Nano* **2008**, *2*, 2356.
[66] Y. Liu, M. Gibbs, J. Puthussery, S. Gaik, R. Ihly, H. W. Hillhouse, M. Law, *Nano Lett.* **2010**, *10*, 1960.
[67] M. V. Kovalenko, M. Scheele, D. V. Talapin, *Science* **2009**, *324*, 1417.
[68] M. Law, M. C. Beard, S. Choi, J. M. Luther, M. C. Hanna, A. J. Nozik, *Nano Lett.* **2008**, *8*, 3904.
[69] N. Zhao, T. P. Osedach, L. Y. Chang, S. M. Geyer, D. Wanger, M. T. Binda, A. C. Arango, M. G. Bawendi, V. Bulovic, *ACS Nano* **2010**, *4*, 3743.
[70] R. T. Ross, A. J. Nozik, *J. Appl. Phys.* **1982**, *53*, 3813.
[71] G. D. Wei, S. R. Forrest, *Nano Lett.* **2007**, *7*, 218.
[72] P. Wurfel, *Physics of Solar Cells: From Principles to New Concepts*, Wiley-VCH, Weinheim **2005**.
[73] M. J. Currie, J. K. Mapel, T. D. Heidel, S. Goffri, M. A. Baldo, *Science* **2008**, *321*, 226.
[74] A. J. Nozik, *Nano Lett.* **2010**, *10*, 2735.
[75] O. Christensen, *J. Appl. Phys.* **1976**, *47*, 689.
[76] R. D. Schaller, M. Sykora, J. M. Pietryga, V. I. Klimov, *Nano Lett.* **2006**, *6*, 424.
[77] V. Sukhovatkin, S. Hinds, L. Brzozowski, E. H. Sargent, *Science* **2009**, *324*, 1542.
[78] V. I. Klimov, *Ann. Rev. Phys. Chem.* **2007**, *58*, 635.
[79] R. D. Schaller, J. M. Pietryga, V. I. Klimov, *Nano Lett.* **2007**, *7*, 3469.
[80] G. Nair, L. Y. Chang, S. M. Geyer, M. G. Bawendi, *Nano Lett.* **2011**, *11*, 2145.
[81] V. I. Klimov, M. Sykora, J. Joo, J. M. Pietryga, *Nano Lett.* **2010**, *10*, 2049.
[82] C. Jundt, G. Klein, B. Sipp, J. Lemoigne, M. Joucla, A. A. Villaeys, *Chem. Phys. Lett.* **1995**, *241*, 84.
[83] M. Pope, N. E. Geacinto, F. Vogel, *Mol. Cryst. Liq. Cryst.* **1969**, *6*, 83.
[84] S. Singh, W. J. Jones, W. Siebrand, B. P. Stoichef, W. G. Schneide, *J. Chem. Phys.* **1965**, *42*, 330.
[85] V. K. Thorsmolle, R. D. Averitt, J. Demsar, D. L. Smith, S. Tretiak, R. L. Martin, X. Chi, B. K. Crone, A. P. Ramirez, A. J. Taylor, *Phys. Rev. Lett.* **2009**, *102*, 017401.
[86] P. M. Zimmerman, Z. Y. Zhang, C. B. Musgrave, *Nat. Chem.* **2010**, *2*, 648.
[87] J. Lee, P. Jadhav, M. A. Baldo, *Appl. Phys. Lett.* **2009**, *95*, 033301.
[88] A. Rao, M. W. B. Wilson, J. M. Hodgkiss, S. Albert-Seifried, H. Bassler, R. H. Friend, *J. Am. Chem. Soc.* **2010**, *132*, 12698.
[89] W. A. Luhman, R. J. Holmes, *Appl. Phys. Lett.* **2009**, *94*, 153304.
[90] P. Jadhav, A. Mohanty, J. Sussman, J. Lee, M. A. Baldo, *Nano Lett.* **2011**, *11*, 1495.
[91] The doubling of the photocurrent has minimal impact on V_{OC} through $\ln(2J_{SC}/J_S)/\ln(J_{SC}/J_S) \approx 1$ for J_s is the SQ limit.
[92] I. Paci, J. C. Johnson, X. D. Chen, G. Rana, D. Popovic, D. E. David, A. J. Nozik, M. A. Ratner, J. Michl, *J. Am. Chem. Soc.* **2006**, *128*, 16546.
[93] Y. Yuan, J. Huang, G. Li, *Green* **2011**, *1*, 65.
[94] A. Hadipour, B. de Boer, P. W. M. Blom, *Org. Elect.* **2008**, *9*, 617.
[95] R. Franke, B. Maennig, A. Petrich, M. Pfeiffer, *Sol. Energy Mater. Sol. Cells* **2008**, *92*, 732.
[96] J. G. Xue, S. Uchida, B. P. Rand, S. R. Forrest, *Appl. Phys. Lett.* **2004**, *85*, 5757.
[97] Y. Yaun, J. Huang, G. Li, *Green* **2011**, *1*, 65.
[98] K. Zweibel, *Sol. Energy Mater. Sol. Cells* **1999**, *59*, 1.
[99] *Annual Energy Review 2009*, U.S. Energy Information Administration, U.S. Department of Energy, Washington, DC **2010**.
[100] Technology Roadmap - Solar Photovoltaic Energy, International Energy Agency, http://www.iea.org/papers/2010/pv_roadmap.pdf **2010, (**p. 1, paragraph 3) (accessed July 2011).
[101] P. Denholm, R. M. Margolis, *Energy Policy* **2007**, *35*, 2852.
[102] *Electric Power Monthly July 2011*, U.S. Energy Information Administration, U.S. Department of Energy, Washington, DC **2011**.
[103] Estimating U.S. Government Subsidies to Energy Sources: 2002-2008. Environmental Law Institute, http://www.eli.org/Program_Areas/innovation_governance_energy.cfm, 2009, (accessed July 2011).
[104] K. Zweibel, The Terawatt Challenge for Thin Film PV, *Technical Report NREL/TP-520-38350*, US Department of Commerce, Springfield, VA **2005.**.
[105] The factor 8760 is the total hours per year; the factor 1000 is to convert \$ W^{-1} to \$ kW^{-1}. The capacity factor, CF, is calculated as the fraction of useful solar illumination hours divided by the hours in a year. Average CF values range from 12% (Maine) to 21% (Phoenix).
[106] J. Kalowekamo, E. Baker, *Sol. Energy* **2009**, *83*, 1224.
[107] J. Poortmans, V. Arkhipov, *Thin Film Solar Cells Fabrication, Characterization and Applications*, John Wiley and Sons Ltd, West Sussex, England **2006**, Ch. 11.
[108] J. Lushetsky, The prospect for \$1/Watt Electricity from Solar, presented at *\$1/W Photovoltaic Systems Workshop*, Washington, DC, Aug. **2010**.
[109] Light intensity dependence of single- and tandem-junction cells needs to be carefully considered to determine the accurate LEC comparison over seasonal and daytime lighting variability not included in this calculation.
[110] M. C. Barr, J. A. Rowehl, R. R. Lunt, J. J. Xu, A. Wang, C. M. Boyce, S. G. Im, V. Bulovic, K. K. Gleason, *Adv. Mater.* **2011**, *23*, 3500.
[111] M. I. Asghar, K. Miettunen, J. Halme, P. Vahermaa, M. Toivola, K. Aitola, P. Lund, *Energy Environ. Sci.* **2010**, *3*, 418.
[112] M. Jorgensen, K. Norrman, F. C. Krebs, *Sol. Energy Mater. Sol. Cells* **2008**, *92*, 686.
[113] M. O. Reese, A. M. Nardes, B. L. Rupert, R. E. Larsen, D. C. Olson, M. T. Lloyd, S. E. Shaheen, D. S. Ginley, G. Rumbles, N. Kopidakis, *Adv. Funct. Mater.* **2010**, *20*, 3476.
[114] J. M. Luther, M. Law, M. C. Beard, Q. Song, M. O. Reese, R. J. Ellingson, A. J. Nozik, *Nano Lett.* **2008**, *8*, 3488.

[115] F. C. Krebs, K. Norrman, *Prog. Photovoltaics* **2007**, *15*, 697.
[116] H. Aziz, Z. D. Popovic, *Chem. Mater.* **2004**, *16*, 4522.
[117] P. E. Burrows, S. R. Forrest, T. X. Zhou, L. Michalski, *Appl. Phys. Lett.* **2000**, *76*, 2493.
[118] Universal Display Corporation PHOLED Features and Performance, http://www.universaldisplay.com/default.asp?contentID = 604. Universal Display Corp. (accessed August, 2011).
[119] S. Jia, M. O. Reese, D. Laird, J. Hauch, Organic Photovoltaic Lifetime Assessment: Recommended Practices, presented at *International Summit On OPV Stability Amsterdam*, April, **2009**.
[120] C. J. Brabec, S. Gowrisanker, J. J. M. Halls, D. Laird, S. J. Jia, S. P. Williams, *Adv. Mater.* **2010**, *22*, 3839.
[121] C. H. Peters, I. T. Sachs-Quntana, J. P. Kastrop, S. Beaupre, M. Leclerc, M. D. McGehee, *Adv. Energy Mater.* **2011**, *1*, 491.
[122] N. Kato, Y. Takeda, K. Higuchi, A. Takeichi, E. Sudo, H. Tanaka, T. Motohiro, T. Sano, T. Toyoda, *Sol. Energy Mater. Sol. Cells* **2009**, *93*, 893.
[123] R. Garcia-Valverde, J. A. Cherni, A. Urbina, *Prog. Photovoltaics* **2010**, *18*, 535.
[124] European Environment Agency. Greenhouse gas emission trends and projections in Europe. Report:No. 5/2008. Office for Official Publications of the European Communities, Luxemborg, 2008.
[125] G. P. Kushto, W. H. Kim, Z. H. Kafafi, *Org. Photovoltaics V* **2004**, *5520*, 118.
[126] C. W. Chu, Y. Shao, V. Shrotriya, Y. Yang, *Appl. Phys. Lett.* **2005**, *86*.
[127] Y. Shao, Y. Yang, *Adv. Mater.* **2005**, *17*, 2841.
[128] J. Wagner, M. Gruber, A. Hinderhofer, A. Wilke, B. Broker, J. Frisch, P. Amsalem, A. Vollmer, A. Opitz, N. Koch, F. Schreiber, W. Brutting, *Adv. Funct. Mater.* **2010**, *20*, 4295.
[129] T. Taima, J. Sakai, T. Yamanari, K. Saito, *Jpn. J. Appl. Phys. Part 2* **2006**, *45*, L995.
[130] D. Fujishima, H. Kanno, T. Kinoshita, E. Maruyama, M. Tanaka, M. Shirakawa, K. Shibata, *Sol. Energy Mater. Sol. Cells* **2009**, *93*, 1029.
[131] M. D. Perez, C. Borek, P. I. Djurovich, E. I. Mayo, R. R. Lunt, S. R. Forrest, M. E. Thompson, *Adv. Mater.* **2009**, *21*, 1517.
[132] F. Yang, K. Sun, S. R. Forrest, *Adv. Mater.* **2007**, *19*, 4166.
[133] B. Verreet, S. Schols, D. Cheyns, B. P. Rand, H. Gommans, T. Aernouts, P. Heremans, J. Genoe, *J. Mater. Chem.* **2009**, *19*, 5295.
[134] Y. Matsuo, Y. Sato, T. Niinomi, I. Soga, H. Tanaka, E. Nakamura, *J. Am. Chem. Soc.* **2009**, *131*, 16048.
[135] D. Wynands, M. Levichkova, M. Riede, M. Pfeiffer, P. Baeuerle, R. Rentenberger, P. Denner, K. Leo, *J. Appl. Phys.* **2010**, *107*, 014517.
[136] W. J. Zeng, K. S. Yong, Z. M. Kam, F. R. Zhu, Y. N. Li, *Appl. Phys. Lett.* **2010**, *97*, 133304.
[137] T. S. Jones, K. V. Chauhan, P. Sullivan, J. L. Yang, *J. Phys. Chem. C* **2010**, *114*, 3304.
[138] N. Li, B. E. Lassiter, R. R. Lunt, G. Wei, S. R. Forrest, *Appl. Phys. Lett.* **2009**, *94*, 023307.
[139] J. D. Zimmerman, V. V. Diev, K. Hanson, R. R. Lunt, E. K. Yu, M. E. Thompson, S. R. Forrest, *Adv. Mater.* **2010**, *22*, 2780.
[140] W. Zhang, R. Zhu, F. Li, Q. Wang, B. Liu, *J. Phys. Chem. C* **2011**, *115*, 7038.
[141] S. Eu, S. Hayashi, T. Umeyama, A. Oguro, M. Kawasaki, N. Kadota, Y. Matano, H. Imahori, *J. Phys. Chem. C* **2007**, *111*, 3528.
[142] T. Bessho, E. C. Constable, M. Graetzel, A. H. Redondo, C. E. Housecroft, W. Kylberg, M. K. Nazeeruddin, M. Neuburger, S. Schaffner, *Chem. Commun.* **2008**, 3717.
[143] M. Thelakkat, C. S. Karthikeyan, H. Wietasch, *Adv. Mater.* **2007**, *19*, 1091.
[144] B. O'Regan, M. Gratzel, *Nature* **1991**, *353*, 737.
[145] H. J. Snaith, A. J. Moule, C. Klein, K. Meerholz, R. H. Friend, M. Gratzel, *Nano Lett.* **2007**, *7*, 3372.
[146] S. Cherian, C. C. Wamser, *J. Phys. Chem. B* **2000**, *104*, 3624.
[147] M. K. Nazeeruddin, A. Kay, I. Rodicio, R. Humphrybaker, E. Muller, P. Liska, N. Vlachopoulos, M. Gratzel, *J. Am. Chem. Soc.* **1993**, *115*, 6382.
[148] C. G. Wu, C. Y. Chen, J. G. Chen, S. Wu, J. Y. Li, K. C. Ho, *Angew. Chem. Int. Ed.* **2008**, *47*, 7342.
[149] J. J. He, G. Benko, F. Korodi, T. Polivka, R. Lomoth, B. Akermark, L. C. Sun, A. Hagfeldt, V. Sundstrom, *J. Am. Chem. Soc.* **2002**, *124*, 4922.
[150] L. Y. Han, Y. Chiba, A. Islam, Y. Watanabe, R. Komiya, N. Koide, *Jpn. J. Appl. Phys. Part 2* **2006**, *45*, L638.
[151] M. D. Irwin, B. Buchholz, A. W. Hains, R. P. H. Chang, T. J. Marks, *Proc. Natl. Acad. Sci. USA* **2008**, *105*, 2783.
[152] K. Vandewal, K. Tvingstedt, A. Gadisa, O. Inganas, J. V. Manca, *Nat. Mater.* **2009**, *8*, 904.
[153] G. J. Zhao, Y. J. He, Y. F. Li, *Adv. Mater.* **2010**, *22*, 4355.
[154] S. H. Park, K. Lee, A. Roy, S. Beaupre, S. Cho, N. Coates, J. S. Moon, D. Moses, M. Leclerc, A. J. Heeger, *Nat. Photonics* **2009**, *3*, 297.
[155] A. P. Zoombelt, S. G. J. Mathijssen, M. G. R. Turbiez, M. M. J. Wienk, R. A. Janssen, *J. Mater. Chem.* **2010**, *20*, 2240.
[156] J. Peet, J. Y. Kim, N. E. Coates, W. L. Ma, D. Moses, A. J. Heeger, G. C. Bazan, *Nat. Mater.* **2007**, *6*, 497.
[157] A. P. Zoombelt, M. Fonrodona, M. G. R. Turbiez, M. M. Wienk, R. A. J. Janssen, *J. Mater. Chem.* **2009**, *19*, 5336.
[158] H. N. Yi, R. G. Johnson, A. Iraqi, D. Mohamad, R. Royce, D. G. Lidzey, *Macromol. Rapid Commun.* **2008**, *29*, 1804.
[159] E. Perzon, F. L. Zhang, M. Andersson, W. Mammo, O. Inganas, M. R. Andersson, *Adv. Mater.* **2007**, *19*, 3308.
[160] A. P. Zoombelt, M. Fonrodona, M. M. Wienk, A. B. Sieval, J. C. Hummelen, R. A. J. Janssen, *Org. Lett.* **2009**, *11*, 903.
[161] A. C. Arango, *Ph.D. Thesis, Massachusetts Institute of Technology, Cambridge, MA* **2010**.
[162] A. C. Arango, D. C. Oertel, Y. F. Xu, M. G. Bawendi, V. Bulovic, *Nano Lett.* **2009**, *9*, 860.
[163] Q. Shen, A. Yamada, S. Tamura, T. Toyoda, *Appl. Phys. Lett.* **2010**, *97*, 123107.
[164] S. Dayal, M. O. Reese, A. J. Ferguson, D. S. Ginley, G. Rumbles, N. Kopidakis, *Adv. Funct. Mater.* **2010**, *20*, 2629.
[165] A. G. Pattantyus-Abraham, I. J. Kramer, A. R. Barkhouse, X. H. Wang, G. Konstantatos, R. Debnath, L. Levina, I. Raabe, M. K. Nazeeruddin, M. Gratzel, E. H. Sargent, *ACS Nano* **2010**, *4*, 3374.
[166] R. Debnath, J. Tang, D. A. Barkhouse, X. H. Wang, A. G. Pattantyus-Abraham, L. Brzozowski, L. Levina, E. H. Sargent, *J. Am. Chem. Soc.* **2010**, *132*, 5952.
[167] P. R. Brown, R. R. Lunt, N. Zhao, T. P. Osedach, D. D. Wanger, L. Y. Chang, M. G. Bawendi, V. Bulovic, *Nano Lett.* **2011**, *11*, 2955.
[168] K. W. Johnston, A. G. Pattantyus-Abraham, J. P. Clifford, S. H. Myrskog, D. D. MacNeil, L. Levina, E. H. Sargent, *Appl. Phys. Lett.* **2008**, *92*, 151115.
[169] P. Wang, S. M. Zakeeruddin, J. E. Moser, M. K. Nazeeruddin, T. Sekiguchi, M. Gratzel, *Nat. Mater.* **2003**, *2*, 498.
[170] D. B. Kuang, C. Klein, S. Ito, J. E. Moser, R. Humphry-Baker, N. Evans, F. Duriaux, C. Graetzel, S. M. Zakeeruddin, M. Graetzel, *Adv. Mater.* **2007**, *19*, 1133.
[171] D. Shi, N. Pootrakulchote, R. Z. Li, J. Guo, Y. Wang, S. M. Zakeeruddin, M. Gratzel, P. Wang, *J. Phys. Chem. C* **2008**, *112*, 17046.
[172] C. Y. Chen, M. K. Wang, J. Y. Li, N. Pootrakulchote, L. Alibabaei, C. H. Ngoc-le, J. D. Decoppet, J. H. Tsai, C. Gratzel, C. G. Wu, S. M. Zakeeruddin, M. Gratzel, *ACS Nano* **2009**, *3*, 3103.
[173] G. L. Zhang, H. Bala, Y. M. Cheng, D. Shi, X. J. Lv, Q. J. Yu, P. Wang, *Chem. Commun.* **2009**, *16*, 2198.
[174] J. A. Hauch, P. Schilinsky, S. A. Choulis, S. Rajoelson, C. J. Brabec, *Appl. Phys. Lett.* **2008**, *93*, 103306.
[175] M. Hermenau, K. Leo, M. Riede, *Org. Photonics IV* **2010**, 7722.
[176] J. A. Hauch, P. Schilinsky, S. A. Choulis, R. Childers, M. Biele, C. J. Brabec, *Sol. Energy Mater. Sol. Cells* **2008**, *92*, 727.